Experimental Investigation of the Hydrodynamic Coefficients of a Remotely Operated Vehicle Using a Planar Motion Mechanism

Juan Julca Avila[1]
Federal University of ABC,
Rua Santa Adélia, 166,
09210-170, Santo André, SP, Brazil
e-mail: juan.avila@ufabc.edu.br

Kazuo Nishimoto
e-mail: knishimo@usp.br

Claudio Mueller Sampaio
e-mail: clasamp@usp.br

Department of Naval Architecture and
Ocean Engineering,
University of São Paulo,
Av. Prof. Mello Moraes, 2231,
05508-900, São Paulo, SP, Brazil

Julio C. Adamowski
Department of Mechatronics Engineering,
University of São Paulo,
Av. Prof. Mello Moraes, 2231,
05508-900 São Paulo, SP, Brazil
e-mail: jcadamow@usp.br

The determination of hydrodynamic coefficients of full scale underwater vehicles using system identification (SI) is an extremely powerful technique. The procedure is based on experimental runs and on the analysis of on-board sensors and thrusters signals. The technique is cost effective and it has high repeatability; however, for open-frame underwater vehicles, it lacks accuracy due to the sensors' noise and the poor modeling of thruster-hull and thruster-thruster interaction effects. In this work, forced oscillation tests were undertaken with a full scale open-frame underwater vehicle. These conducted tests are unique in the sense that there are not many examples in the literature taking advantage of a PMM installation for testing a prototype and; consequently, allowing the comparison between the experimental results and the ones estimated by parameter identification. The Morison's equation inertia and drag coefficients were estimated with two parameter identification methods, that is, the weighted and the ordinary least-squares procedures. It was verified that the in-line force estimated from Morison's equation agrees well with the measured one except in the region around the motion inversion points. On the other hand, the error analysis showed that the ordinary least-squares provided better accuracy and, therefore, was used to evaluate the ratio between inertia and drag forces for a range of Keulegan–Carpenter and Reynolds numbers. It was concluded that, although both experimental and estimation techniques proved to be powerful tools for evaluation of an open-frame underwater vehicle's hydrodynamic coefficients, the research provided a rich amount of reference data for comparison with reduced models as well as for dynamic motion simulation of ROVs. [DOI: 10.1115/1.4004952]

Keywords: least-square method, Morison's equation, open-frame underwater vehicle, planar motion mechanism.

1 Introduction

Remotely operated vehicles (ROVs) are getting more and more important in underwater environment exploration and exploitation because of their capabilities for environment identification and maintenance support for complex deep water tasks. However, as cited in Ref. [1], the "lack of experimentally validated mathematical models," which is an essential requirement for reliable control system design and implementation of training simulators, has been hindering the development of model-based dynamic positioning technologies.

In the last two decades, ROV hydrodynamic models have been evaluated by two distinct approaches: Model tests in towing tanks, and system identification (SI). The first approach is based on traditional naval architecture procedures relying on planar motion mechanism (PMM) equipped facilities. Besides cost and time disadvantages, this approach suffers from scale effects on the estimated hydrodynamic coefficients. On the other hand, the SI approach corresponds to the analysis of the input/output data obtained from the on-board sensors and the thrusters force inputs during free running trials. This last procedure has usually been applied to low cost evaluation of ROV hydrodynamic models [1–3], however, it has been verified that its results are not very accurate [4] due to intrinsic sensor noise as well as to the poor modeling of the propeller characteristics and its propeller-propeller and propeller-hull interactions.

This article describes and discusses the results of forced oscillation tests carried out with an open-frame prototype ROV using the PMM facility in the Technological Research Institute of Sao Paulo (IPT). The main research objective was to acquire an insight on hydrodynamic coefficient trends as a function of Keulegan–Carpenter and Reynolds numbers.

2 ROV Mechanical Design

The underwater vehicle used in the tests is an open-frame ROV called LAURS. The LAURS was developed and built i the Laboratory of Sensors and Actuators at the University of Sao Paulo (Brazil) to serve as an experimental test platform for research on underwater vehicle dynamics, control, and navigation. The vehicle has been conceived to provide inspection and intervention capabilities for deep water oil field missions.

The LAURS is intrinsically stable in pitch and roll and its station-keeping is guaranteed by eight dc brushless electric thrusters. The vehicle's general layout (Fig. 1) is composed of an aluminum tubular box structure, 1.4 m long × 1.2 m wide × 0.9 m high, supporting three equal pressure vessels of 1.0 m long and

[1]Corresponding author.

Contributed by the Ocean Offshore and Arctic Engineering Division of ASME for publication in the JOURNAL OF OFFSHORE MECHANICS AND ARCTIC ENGINEERING. Manuscript received July 2, 2009; final manuscript received April 18, 2010; published online December 2, 2011. Assoc. Editor: Elzbieta Maria Bitner-Gregersen.

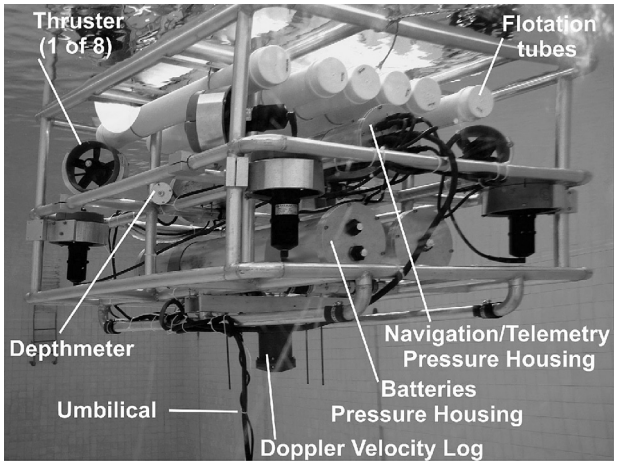

Fig. 1 LAURS general layout

0.17 m diameter. Its air weight and volume displacement (buoyancy) force are around, respectively, 189 kg and 35 N. The vehicle is arranged in two parts; the upper part containing PVC tubes for buoyancy control (flotation tubes), the electronics/sensors (navigation/telemetry) containment pressure housing, and four horizontal thrusters; while the bottom part includes two battery pressure housings and four vertical thrusters. Modular structural components allow the LAURS to be easily reconfigured in agreement with specific tasks. The vehicle has been equipped with a variety of navigation sensors, including Doppler velocity log, fiber-optic gyroscope, digital altimeter, compass, and tilt and depth measuring devices.

3 Modeling and Parameter Identification Method

Morison's equation was originally proposed to describe the horizontal hydrodynamic forces generated by progressive waves on slender tubular pipelines or jacket structural members. Its basic assumption was that the wave properties would not be affected by the structure and that the resulting force could be decomposed as the sum of an inertia term (due to the fluid acceleration) and a drag term (due to the fluid velocity) [5]. In spite of its original application, Morison's equation was adopted for representing loadings on an underwater vehicle with the understanding that the hydrodynamic coefficients should be experimentally determined for each particular test condition. In this work the authors applied Morison's equation for describing the in-line forces resulting from the oscillatory motion imposed on the underwater vehicle by a PMM installation. The expression is given by

$$f(t) = \frac{1}{2}\rho C_D A_p u(t)|u(t)| + (C_M \rho \forall + m)\dot{u}(t) \tag{1}$$

where $f(t)$ is the in-line force acting on the vehicle; $u(t)$ and $\dot{u}(t)$ are the vehicle's velocity and acceleration, respectively; C_D and C_M are the drag and inertia coefficients; A_p is the projected area in the motion's direction; $\forall$ is the volume of the fluid displaced by the vehicle; m is the vehicle's dry mass; and ρ is the water density. It is important to explain that the velocity and acceleration terms in Eq. (1) correspond to the vehicle's absolute velocities and accelerations as the experimental tests were performed without current. The first term on the right-hand side of Eq. (1) is the sum of viscous and form drag produced by the velocity relative between the structure and the fluid and is modeled as being proportional to the square of the relative velocity. The second term considers the force of inertia due to both the added mass and rigid body and is modeled as being proportional to the acceleration of the vehicle.

In this work, in order to consider only the hydrodynamic forces due to the vehicle's motion, the contributions of both the vertical beam used for towing the vehicle as well the vehicle's inertia were subtracted from the measured force, as detailed in Sec. 5.2. Therefore, the final equation including only hydrodynamic components is expressed by

$$\begin{aligned} f(t) &= \frac{1}{2}\rho C_D A_p u(t)|u(t)| + C_M \rho \forall \dot{u}(t) \\ &= C_D k_D u(t)|u(t)| + C_M k_I \dot{u}(t) \end{aligned} \tag{2}$$

where $f(t)$ is the in-line force acting on the vehicle due to the hydrodynamic effects only, and $k_D = \frac{1}{2}\rho A_p$ and $k_I = \rho \forall$. Equation (2) is composed of the drag force, f_D, and the inertia force, f_I, which are expressed by

$$\begin{aligned} f_D &= \frac{1}{2}\rho C_D A_p u(t)|u(t)| \\ f_I &= C_M \rho \forall \dot{u}(t) \end{aligned} \tag{3}$$

In this work the C_D and $C_M$coefficients of Eq. (2) were experimentally identified from measured data of force, velocity, and acceleration. The Section 3.1 describes the parameter identification method used to determine the C_D and $C_M$coefficients of Eq. (2).

3.1 Parameter Identification Method. The methods used to analyze experimental data in terms of Morison's equation parameters have a significant effect on both the drag and inertia coefficients and on the equation's predictive capacity. A wide variety of approaches, both in time and in frequency domain, has been studied; a careful assessment was made by Wolfram and Naghipour [6] for the circular cylinder in the case of waves. The authors found that there was no single method accurate enough for all circumstances but the weighted least squares method produced, on average, both the lowest bias and the lowest root mean square error. On the basis of that article, the present authors have chosen to evaluate three identification methods: weighted least-square (WLS), ordinary least-square (OLS) and Fourier average. Conversely, Avila [4] had observed that the C_D and C_M coefficients generated by the OLS method closely agreed with those produced by the Fourier average method but showed meaningful deviations when compared to those given by the WLS method. As a result of this fact, the results of the Fourier average method will not be discussed in this article.

3.1.1 Weighted Least-Squares Method. The application of the WLS method for estimating C_D and C_M relies on the minimization of a scalar cost function, J, which should be conveniently chosen. As suggested by Sarpkaya et al. [8], the cost function J is defined by

$$J = \sum_{k=1}^{N} f_m^2(t_k)[f_m(t_k) - f(t_k)]^2 \tag{4}$$

where $f_m(t_k)$ is the in-line force measured in the discrete time instant t_k, $f(t_k)$ is the in-line force calculated from Morison's equation give by Eq. (2), and $N$is the number of samples of measured force time series. The function J is composed of a weighted summation of squares of prediction errors $\varepsilon(t_k)$, which corresponds to the difference between the measured and the calculated force, i.e.,

$$\varepsilon(t_k) = f_m(t_k) - f(t_k) \tag{5}$$

The term $f_m^2(t_k)$ in Eq. (4) represents the weighting factor and was selected due to the fact that there is great interest in predicting maximum forces. Thus, it is guaranteed that the measured higher

values points in the force time series have more weight on the C_D and C_M determination.

The drag and inertia coefficients are obtained by imposing the minimization of the cost function, J, and solving, simultaneously, Eqs. (6) and (7).

$$\frac{\partial J}{\partial C_M} = f_m^2 k_D C_D \sum u|u|\dot{u} + f_m^2 k_I C_M \sum \dot{u}^2 - \sum f_m^3 \dot{u} = 0 \quad (6)$$

$$\frac{\partial J}{\partial C_D} = f_m^2 k_D C_D \sum u^4 + f_m^2 k_I C_M \sum u|u|\dot{u} - \sum f_m^3 u|u| = 0 \quad (7)$$

The final expressions for both coefficients are shown in the following equations

$$C_D = \frac{\sum f_m^3 u|u| \sum f_m^2 \dot{u}^2 - \sum f_m^3 \dot{u} \sum f_m^2 u|u|\dot{u}}{k_D \left\{ \sum f_m^2 u^4 \sum f_m^2 \dot{u}^2 - \left(\sum f_m^2 \dot{u} u|u|\right)^2 \right\}} \quad (8)$$

$$C_M = \frac{\sum f_m^3 \dot{u} \sum f_m^2 u^4 - \sum f_m^3 u|u| \sum f_m^2 \dot{u} u|u|}{k_I \{ \sum f_m^2 \dot{u}^2 \sum f_m^2 u^4 - \left(\sum f_m^2 \dot{u} u|u|\right)^2 \}} \quad (9)$$

3.1.2 Ordinary Least-Squares. Similar to the WLS method, the adopted cost function of the OLS method has the same general form as depicted in Eq. (4) but with a weighting factor of unit constant value. As a consequence, the OLS method assumes that all data points of the measured force time series have the same weight on the estimation of C_D and C_M, whose expressions, derived by the same minimization procedure as described in 3.1.1, are given by

$$C_D = \frac{\sum f_m u|u| \sum \dot{u}^2 - \sum f_m \dot{u} \sum u|u|\dot{u}}{k_D \left\{ \sum u^4 \sum \dot{u}^2 - \left(\sum \dot{u} u|u|\right)^2 \right\}} \quad (10)$$

$$C_M = \frac{\sum f_m \dot{u} \sum u^4 - \sum f_m u|u| \sum \dot{u} u|u|}{k_I \{ \sum \dot{u}^2 \sum u^4 - \left(\sum \dot{u} u|u|\right)^2 \}} \quad (11)$$

4 Experimental Facilities and Procedures

The forced oscillation and stationary-state tests in still water were carried out in the towing tank at the Ship and Ocean Engineering Center of the Technological Research Institute of São Paulo. The facility has a 280 m long continuous towing rail system with two transverse section portions; the 60 m short stretch, 4.6 m wide and 4 m deep; and the 220 m long one with a breadth and a depth of 6.0 m each. The test program was performed using the PMM carriage connected to the main towing one. The PMM system was designed for testing ships and ocean platform models; it has maximum oscillation amplitude of ± 1.0 m and a limit load capacity of 2000 N. The functioning mechanism consists of a horizontal screw shaft driven by two on-board servo-controlled electric motors that, moving the small sub-carriage block, produces the transverse displacement. Attached to the sub-carriage block and aligned in the vertical direction there is an electric motor for the yawing motion.

The LAURS was rigidly fixed to the sub-carriage through a 28.8 kg steel tubular cylindrical bar with a length of 1000 mm and a diameter of 76.8 mm. The depth of the top of the vehicle's structure was of 900 mm. Figure 2 shows the LAURS experimental setup for the PMM tests. A high-speed camera system (Qualisys) was employed for the determination of the LAURS position. The system works with a stroboscopic unit emitting short light pulses, retro-reflective markers (10 mm diameter spheres) attached to the vehicle, and cameras for registering the reflected signal. With cameras of 2 MP resolution, the advanced tracking/analysis software provides the position with ± 2 mm precision as well as the velocity and the acceleration in a user defined reference frame. On the other hand, the force measuring arrangement was made up of a number of strain gauges attached to the supporting bar lower end whose signals were fed to a 10 mV sensitivity amplifier to obtain load measures of high accuracy. Subsequently, the signals were stored on a personal computer in data form.

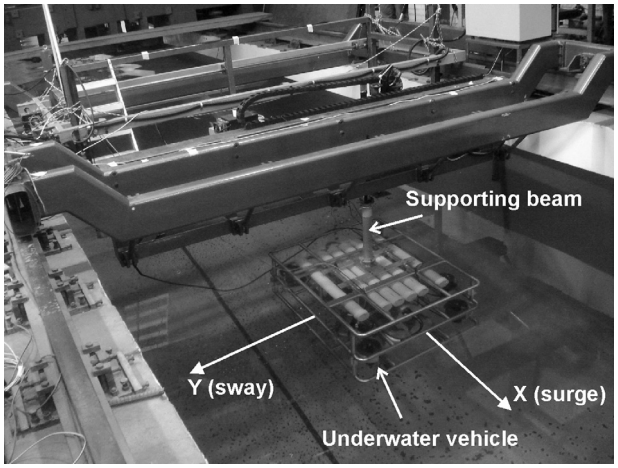

Fig. 2 The planar motion mechanism and the experimental setup. The picture shows the LAURS during the tests in sway.

The experimental data were acquired with a 200 Hz sampling frequency and were filtered with a fifth-order Butterworth low pass filter with a cut frequency of 1 Hz. Finally, as the experimental setup includes the supporting beam and the vehicle's inertia effects on the measured forces, their contributions were subtracted from the measured forces by the procedure explained in Sec. 5.2.

5 Results and Discussions

This section starts by describing the nondimensional numbers as well as the predictive capacity parameters of Morison's equation, which are used in the analyses of results. Following is a discussion of the procedures for discounting the effects of the supporting bar. Finally, the results of the PMM tests are presented and discussed.

5.1 Nondimensional Numbers and Performance Parameters. In this work the C_D and $C_M$coefficient values are estimated for different Keulegan–Carpenter numbers, KC, and Reynolds numbers, Re. These nondimensional parameters that characterize the viscous flow phenomena and, therefore, the drag force relevance on the vehicle dynamics, are defined as

$$KC = \frac{U_m T}{L_c}$$
$$\mathrm{Re} = \frac{U_m L_c}{\nu} \quad (12)$$

where U_m is the motion's maximum velocity amplitude, T is the oscillation period, $L_c$is a characteristic length of the vehicle, and ν is the water kinematic viscosity.

Two parameters were chosen to assess how well Morison's equation [Eq. (2)] represents the measured forces. The first parameter, E, is based on the difference between the measured maximum force,$f_m^{\max}$, and the calculated maximum force, $f^{\max}$, in a wave cycle and is defined as

$$E = \frac{f_m^{\max} - f^{\max}}{f_m^{\max}} 100\% \quad (13)$$

The second parameter, which measures the mapping quality for all points of the time force series, is the mean of the absolute error between measured and Morison's calculated forces and is given by

$$e = mean(|f_m - f|) \quad (14)$$

Besides, in order to verify whether the flow regime is dominated by the drag or the inertia term, the authors defined the ratio of the absolute values of the drag force and the inertia force as

$$\lambda = \frac{\sum_{k=1}^{N} |f_D(t_k)|}{\sum_{k=1}^{N} |f_I(t_k)|} \tag{15}$$

where f_D and f_I are, respectively, the drag force and inertia force as given in Eq. (3).

5.2 Discounting the Effects of the Supporting Beam. As already explained, in order to identify the C_D and C_M coefficients of the model of Eq. (2), the effects of the supporting beam and of the vehicle's inertia had to be subtracted from the measured force. For this purpose, the following expression was introduced to estimate the in-line force assigned only to the hydrodynamic loading on the vehicle:

$$f_m^H = f_m - \tfrac{1}{2}\rho C'_D A'_p u|u| - (C'_M \rho \forall' + m')\dot{u} - m\dot{u} \tag{16}$$

The first term on the right-hand side is the measured force; the second and third terms represent, respectively, the estimated drag and inertia forces of the supporting beam; and the fourth term is the vehicle's inertia force. The selected parameters of the supporting bar are $C'_D = 0.85$, $C'_M = 1$, $A'_p = 0.076\text{m}^2$, $\forall' = 4.59 \times 10^{-3}\text{m}^3$, and $m' = 28.8\text{kg}$, where the prime symbol is used for indicating supporting beam values.

5.3 Results. A series of experimental forced oscillation trials in surge has been undertaken with varying parameters (amplitude and period). Six amplitudes were tested, 50 mm, 100 mm, 200 mm, 300 mm, 400 mm, and 500 mm; each one with different periods, from 6 s to the 30 s maximum. As an example, Fig. 3 shows the acquired data for the 400 mm and 8 s amplitude and period case. It is interesting to observe that, in the upper diagram [Fig. 3(*a*)], the sway measured in-line force, F_y, is approximately zero, a result that can be explained by the LAURS geometrical transverse symmetry. On the other hand, Fig. 4 depicts the in-line force components in accordance with Eq. (16) for the test in consideration.

The authors employed both OLS and WLS methods for calculating the C_D and C_M coefficients; the experimental input data for the parameter identification algorithms being the in-line force f_m^H, the velocity u, and the acceleration $\dot{u}$. The variable f_m^H was estimated using Eq. (16), u was obtained by numerical differentiation

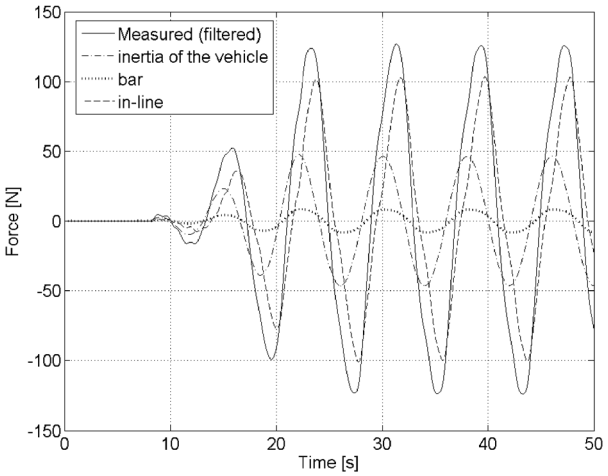

Fig. 4 Forced oscillation test: experimental measured force (filtered) and in-line force

of the position signal and then filtering it with a noncausal Savitzky–Golay polynomial filter, and $\dot{u}$ was obtained by numerical differentiation of the velocity and also using a Savitzky–Golay filter. The velocity and acceleration data provided by the camera motion capture system was not considered in this work because the need for a different algorithm for signal filtering. Furthermore, as an accuracy check for any signal delay caused by the filtering, the velocity response was integrated and the resulting position compared with the original data. Finally, regarding the data string for the application of the parameter identification procedure, two forced oscillation cycles were selected by visual inspection.

In the present work the "quality" of the identified vehicle's coefficients was evaluated by quantitatively comparing the experimentally measured in-line force to that calculated by Morison's equation [Eq. (2)]. This comparison is shown in the bottom diagram of Fig. 5, in which the calculated and the LAURS measured in-line forces [Eq. (16)] are depicted. It can be observed that the in-line force distributions agree very well over most of the time span except around the inflection points. Besides, for the interval between 47 s and 49 s, both OLS and WLS estimating procedures provide in-line forces almost perfectible coalescing with the measured ones. On the other hand, for the 45.8 s time instant, the in-line forces derived from the OLS and WLS parameter

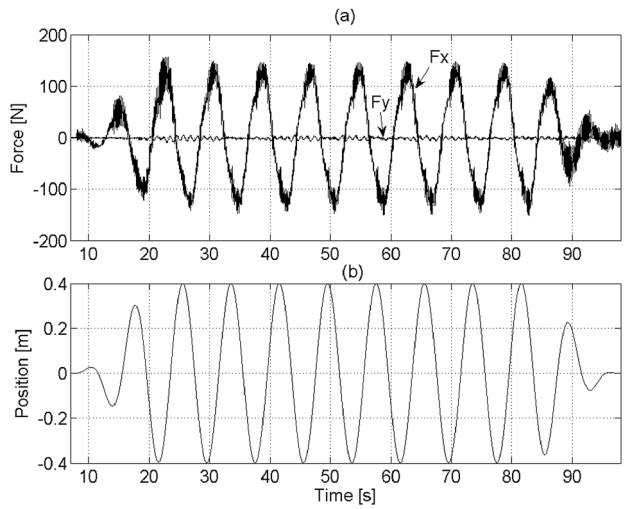

Fig. 3 Forced oscillation experimental results for amplitude of 400 mm and period of 8 s: (*a*) force and (*b*) position

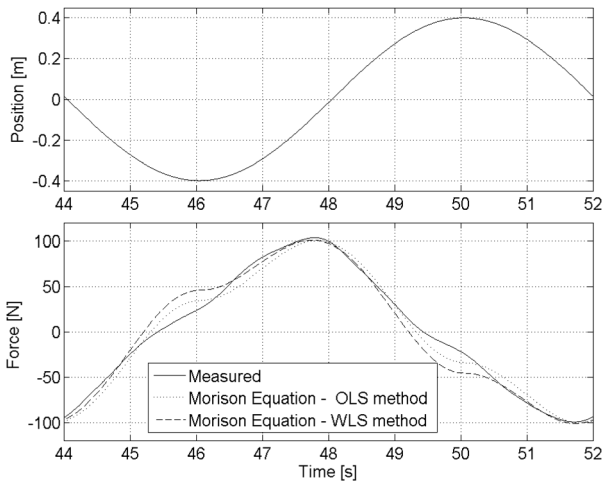

Fig. 5 Comparison of the measured and the Morison's equation calculated in-line forces for the 400 mm amplitude and 8 s period test condition

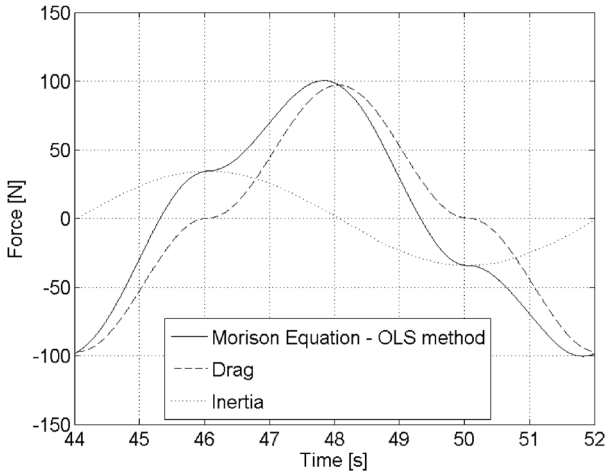

Fig. 6 Drag, inertia and Morison's equation forces for the 400 mm and 8 s test case

identification methodologies have prediction errors of 12.7% and and 23.7% to the measured in-line force, respectively.

The authors observed in the experiments that, around the region of the motion's inflection points, the residue, defined as the difference between the measured and calculated forces, is a significant percentage of the maximum force. This observation was also verified by Sarpkaya [9] in his extensive studies on forces affecting cylinders in oscillatory flows. He added a third term to Morison's equation in order to model the third harmonic of the residue function, which resulted in a significant reduction of the residue. Considering Sarpkaya's improved results, the authors concluded that a modified form of Morison's equation should be considered if the minimization of the ROV's in-line force residue is sought.

Figure 6 shows the time variation of the drag, inertia, and Morison's equation forces for one oscillation cycle where the nonlinear drag behavior can be clearly observed near the abscissa axis. It can be observed that, while the inertia component is maximum (maximum absolute acceleration) at the inflection points, the maximum value of the drag component occurs around the peak of Morrison's force. The parameter λ [Eq. (15)] for this example is equal to 1.62; meaning that the flow regime is dominated by the viscous drag component. This λ value was calculated using the hydrodynamic coefficients obtained with the OLS method. The mean absolute error e [Eq. (14)] obtained using the OLS method was smaller (7.09 ± 4.25 N) than the one obtained with the WLS method (8.09 ± 8.38 N). Finally, the error E [Eq. (13)] obtained in the prediction of peak forces was 3.4% with the OLS method.

The values of the drag-to-inertia ratio (λ), for all the experimental conditions, are shown in the upper diagram of Fig. 7. It can be observed that the drag force is, on average, 1.55 times the inertia

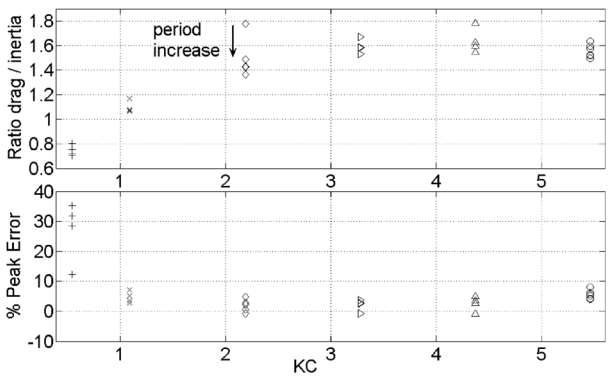

Fig. 7 (Top) Variation of the drag to inertia force ratio and (bottom) prediction error of the peaks of force

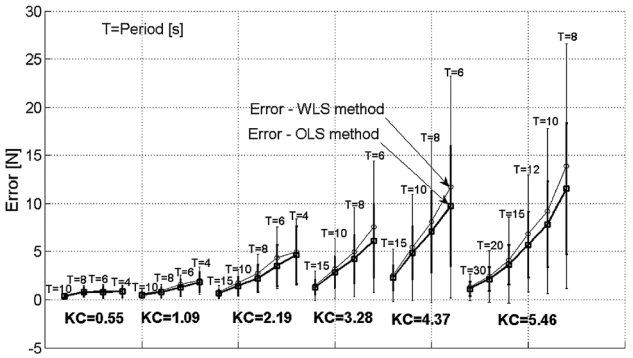

Fig. 8 Mean absolute error obtained by fitting the Morison's equation to the experimental data

component for KC values varying from 2.19 to 5.46 with low dispersion for any specific KC. Besides, in the lower diagram of Fig. 7, the calculated error parameter, E, of the predicted peak forces is smaller than 9% for the whole KC range, except the lowest value ($KC = 0.55$) where the error increases with oscillation period, with 35% error for the 10 s highest period. The reason for this behavior was the measuring system's low signal-to-noise ratio where the vehicle's dry weight requirement of large capacity transducers made nearly impossible the measurement of very small forces. The values of both diagrams were obtained considering the values of the hydrodynamic coefficients obtained by applying the OLS method because of its good performance in spite of the fact that, as already expected, the WLS method has a slight better performance in predicting the force peaks. This conclusion was further checked by comparing the mean absolute error, e, obtained by applying both OLS and WLS parameter identification methodologies. As depicted in Fig. 8, the application of the OLS method resulted in smaller e values for the whole range of KC values; therefore, assuring the authors' decision to adopt it for all calculated quantities.

The estimated values of the drag and inertia coefficients as function of Reynolds number, for different KC numbers, are shown in Figs. 9 and 10. According to these figures, the coefficients C_D and C_M do not depend strongly on the Reynolds number, but, have a clear dependency on the Keulegan–Carpenter number. As depicted in Fig. 9, decreasing KC numbers increase the drag coefficients, C_D, in such a way that, for KC and

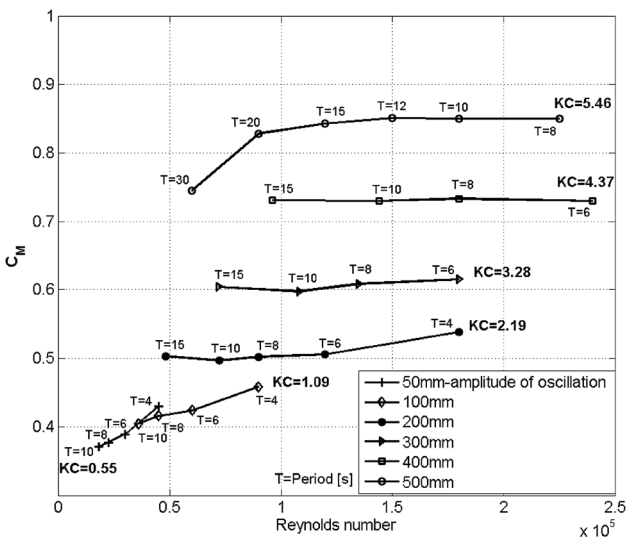

Fig. 9 Drag coefficient for the LAURS in different Keulegan–Carpenter and Reynolds numbers. Motion direction: surge.

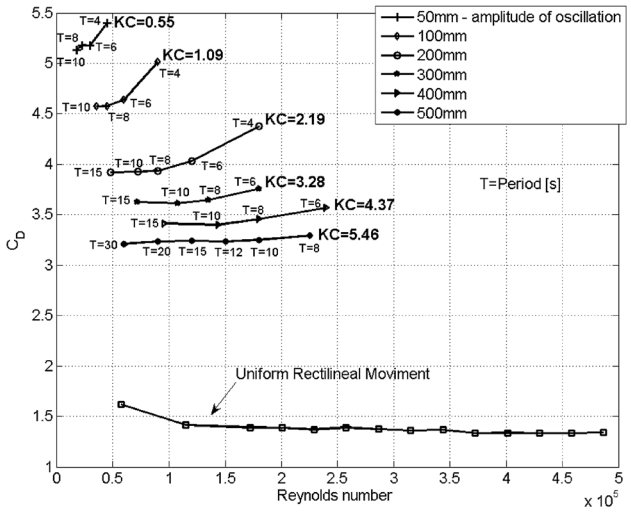

Fig. 10 Inertia coefficient for the LAURS in different Keulegan–Carpenter and Reynolds numbers. Motion direction: surge

oscillation period equal to, respectively, 0.55 and 4 s, the coefficient C_D takes its maximum value of 5.4. Therefore, one would initially say that, for the smallest *KC* value, the drag force would be more important than the inertia force, which, however, according to the upper diagram of Fig. 7, would be just the opposite. In other words, the drag coefficient has not much influence on the in-line force at low *KC* values but, on the other hand, a small change in the inertia coefficient would significantly influence the in-line force.

Finally, in order to determinate the drag coefficient for constant velocities, a series of towing trials was undertaken whose results are plotted in Fig. 9. Besides the fact that the drag coefficient does not depend on the tested range of Reynolds numbers, it could be argued that the average drag coefficient tends to the steady-state value ($C_D = 1.38 \pm 0.072$) with increasing *KC* numbers.

6 Conclusions

This article starts by describing the PMM experimental tests of the open-frame underwater vehicle LAURS, evaluates two parameter identification procedures for the estimation of Morison's equation drag and inertia coefficients, and finally, analyzes the obtained results as a function of Keulegan–Carpenter and Reynolds numbers. The position and the in-line force time series were measured and filtered during the experiments and, subsequently, used as input data to carry out the Weighted Least-Squares and the Ordinary Least-Squares procedures for identifying the drag and inertia coefficients. The maximum obtained *KC* number was 5.46 with *Re* numbers varying from 1.8×10^4 to 2.4×10^5. The main conclusions from this investigation can be summarized as follows:

1. The experimental testing of the LAURS open-frame underwater vehicle in a PMM facility and the estimation of important parameters by parameter identification techniques proved to give good and coherent results. It is important to observe that there are only a few works in the literature describing the identification of Morison's equation coefficients for open-frame underwater vehicles.
2. The expression of Morison's equation given by Eq. (2) provides good accuracy for representing the oscillatory motion of an open-frame underwater vehicle. The in-line forces estimated by the OLS identification method were found to compare very well to the measured ones.
3. The evaluation of the prediction error, *e*, of the in-line forces showed that the OLS method outperforms the WLS method for the determination of the Morison's equation drag and inertia coefficients.
4. The estimated drag and inertia coefficients showed a smooth variation without much scatter. Although the drag coefficient decreases with increasing *KC* number, the inertia coefficient has a direct dependency.
5. The LAURS drag coefficients are large at low *KC* numbers, decreasing sharply with its increase.
6. It has been verified that the drag coefficient of the steady forward motion is independent of the advance velocity for the whole range of Reynolds numbers.

Acknowledgment

The authors would like to thank the FINEP for financial support through the CTPetro/ANP program, the CNPq for scholarship and financial support, the FAPESP for scholarship support, the CENPES/PETROBRAS for the logistic support, and the Ship and Ocean Engineering Center of the Institute of Technologic Research of São Paulo.

References

[1] Smallwood, D., and Whitcomb, L., 2003, "Adaptive Identification of Dynamically Positioned Underwater Robotic Vehicles," IEEE Trans. Control Syst. Technol., **11**(4), pp. 505–515.
[2] Caccia, M., Indiveri, G., and Veruggio, G., 2000, "Modelling and Identification of Open-Frame Variable Configuration Underwater Vehicles," IEEE J. Ocean. Eng., **25**(2), pp. 227–240.
[3] Ridao, P., Tiano, A., El Fakid, A., Carreras, M., and Zirilli, A., 2004, "On the Identification of Non-Linear Models of Unmanned Underwater Vehicles," Control Eng. Pract., **12**, pp. 1483–1499.
[4] Avila, J. P., 2008, "Modelling and Identification of Hydrodynamic Parameters of an Underwater Robotic Vehicle" (in Portuguese), Ph.D. thesis, Polytechnic School of the University of São Paulo, Brazil.
[5] Patel, M. H., *Dynamics of Offshore Structures*, (Butterworth, London, 1989, Chap. 5.
[6] Wolfram, J., and Naghipour, M., 1999, "On the Estimation of Morison Force Coefficients and Their Predictive Accuracy for Very Rough Circular Cylinders," Appl. Ocean Res., **21**, pp. 311–328.
[7] Chakrabarti, S., 2005, *Handbook of Offshore Engineering*, Elsevier Science, Amsterdam, The Netherlands, Chap. 4.
[8] Sarpkaya, T., and Isaacson, M., 1981, *Mechanics of Wave Forces on Offshore Structures*, Van Nostrand, New York, Chap. 3.
[9] Sarpkaya, T., 1981, "A Critical Assessment of Morison's Equation and Its Applications," Proceedings of the International Conference on Hydrodynamics in Ocean Engineering, Trondheim, Norway, pp. 447–467.